DOI: 10.24427/978-83-66391-87-1_02

Cezary MAJ[1], Jacek NAZDROWICZ[1], Adam STAWIŃSKI[1]

2. FRINGING FIELD MODELLING IN MEMS CAPACITIVE COMB-DRIVE ACCELEROMETERS

Modelling is a crucial step in designing MEMS devices. It is needed to estimate the device performance without its fabrication. Initially, simple calculations are needed to verify the possibility of device production with a given performance and to know the basic parameters necessary to achieve the desired goals. Further, optimization is commonly performed in order to improve the design. Both steps require simulation methods that are very fast and precise enough to reduce time to market. In many cases, classical, precise FEM simulations are not necessary and simple analytical models are used. MEMS devices like accelerometers, commonly uses elements of simple shapes that can be easily described with simple analytical formulas. However, analytical modelling is getting more complicated in case of capacitive transduction. Typically, these devices operate in the range of linear response but nothing can be done to avoid the influence of non-uniform electric field. Due to fringing field, a capacitance is often underestimated when using classical parallel plate formula. Therefore, there is a need for proper fringing field modelling. In this chapter, analytical modelling of fringing field on an example of MEMS accelerometer is presented. Specific structure type known as comb-drive consists of many small capacitors that enhance the impact of fringing field. Accelerometers in all axes are analyzed. Moreover, Z-axis accelerometer induces different electric field distribution due to the use of thinned fingers. Thus, analytical formulas are derived for various conditions. Finally, the model is compared with Coventor MEMS+ and fabricated strictures are measured in order to validate analytical approach.

2.1. INTRODUCTION

Accelerometers are one of the most popular devices in the world. They are used in the measurement of angular and linear acceleration of vehicles, machines and other devices

[1] Lodz University of Technology, Poland

used e.g., in inertial navigation [1]. Ever since MEMS technology appeared in the market, the production of MEMS accelerometers continues to grows every year. Due to miniaturization, they are used in almost any mobile devices in detection of spatial orientation and its function controlling with movement [2]. One estimates that there are dozens of accelerometers per person. The most attractive are the capacitive accelerometers due to their high sensitivity, low power consumption and low temperature dependence [3]. Although, the principle of operation remains the same as that of *old-type* sensors, modelling and simulation steps are still necessary to obtain the desired performance. In addition, proper design path allows the shortening of time to market and reduction in the cost of development.

One of the most common and reliable method used during the conception phase is FEM (finite element method) simulation [4]. Three-dimensional model of the sensor is built with desired precision and subsequently divided into nodes (meshing process). Each node is described with equations (the number depends on used types of domains) that are usually differential. Therefore, the complexity of the model influences the number of equations that needs to be solved. Even though the computing power of today's computer is very high, simulation may take longer time to give result. This is particularly noticeable in optimization process. Thus, a faster approach is desirable. Note that during the initial design phase, the designer needs the basic information about the possibility of creating a sensor with imposed parameters. Thereafter, the designer needs the information of the range of sensor dimensions and basic performance (needed for read-out circuit). The use of FEM simulation seems to be unreasonable as it requires the creation of a 3-D model which is time consuming.

An alternate approach is to use analytical modelling [5]. The device is considered as one element and a few analytical equations are formed to describe its behavior. In general, these equations have simplified form e.g., approximated solution of differential equation. Therefore, the solution is very fast and it may be performed without any dedicated software (e.g., with the use of spreadsheet). Moreover, this model can be simply parametrized and used for devices of almost any shape and any dimensions and also used in optimization phase [6, 7]. Note that simplified models are mostly used in devices with regular and simple shapes to obtain high precision. Nevertheless, final product should be verified with FEM simulation in order to obtain the results that takes into account all possible factors omitted in the analytical model.

The need for a simpler and faster models create demand for a software that combines the advantages of analytical modelling (simulations time) and FEM (precision, complex shapes). One of the most promising is Coventor MEMS+ that allows simulating many popular MEMS devices like accelerometers, gyroscopes, microphones, micro-switches, micro-mirrors etc. It still uses meshing but not in a conventional way. Therefore, the simulations are hundred times faster than FEM simulators with very high precision. It should be mentioned that MEMS+ does not allow simulating complex structures but this inconvenience does not reduce its functionality. It has built-in shapes that are commonly used in MEMS devices, typical feature used in analytical models. Moreover, MEMS+ is integrated with other Coventor packages and provides designing of MEMS devices with

IC circuits and packaging. The model can also be exported to Cadence environment in order to perform full IC simulation and automatic layout generation.

Accelerometers are simple devices that can be described with analytical model. They consist of elements of basic shapes where movement and deformation are described with well-known basic formulas. Combining mechanical domain with others needed for describing the type of transduction (electrical, piezoelectric, piezoresitive) is an effortless task. Sometimes, iterative calculations are required however, set of equations have polynomial form which makes it easier to solve. The only factor that affects the accuracy of calculations is the model reduction by omitting certain phenomena. In our consideration, capacitive accelerometers are analyzed. Transduction that uses electric field cannot be simply described with one formula. Fringing fields are underestimated in case of commonly used parallel plate capacitor equation. If accelerometer is a comb-drive type, the accuracy of calculation results are insufficient. In this chapter, we will show how to model fringing field accurately in capacitive comb-drive accelerometers.

2.2. MODELLING OF COMB-DRIVE ACCELEROMETER

2.2.1. PRINCIPLE OF OPERATION

Inertial MEMS accelerometers consist of a proof-mass that is suspended with springs attached to a fixed frame as shown in Fig 2.1.

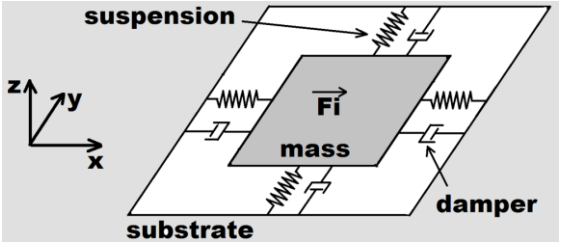

Fig. 2.1. Schematic of MEMS accelerometer

When acceleration is applied, the inertia force acts on the proof-mass causing its displacement from initial position. Springs allows to counteract the inertia force in order to get to equilibrium state. Proper design of springs allows sensing the acceleration in desired direction. The proof-mass moves in *XY* plane in case of *XY*-axis accelerometer and moves in *Z* direction in case of *Z*-axis accelerometer. Capacitive transduction uses a capacitor formed with the proof-mass and fixed part of the sensor. Therefore, two types of accelerometers are used depending on the sensing axis (Fig. 2.2). *XY*-axis accelerometers use comb-drive structure that increases the effective area of capacitor plates [10]. *Z*-axis accelerometers typically use parallel plate structure wherein, bottom plate is placed beneath the proof-mass [10]. Nevertheless, in some cases, comb-drive structures are also used due

to technological restrictions. In both cases, proof-mass movement causes capacitance change that is converted into electrical signal with read-out circuit.

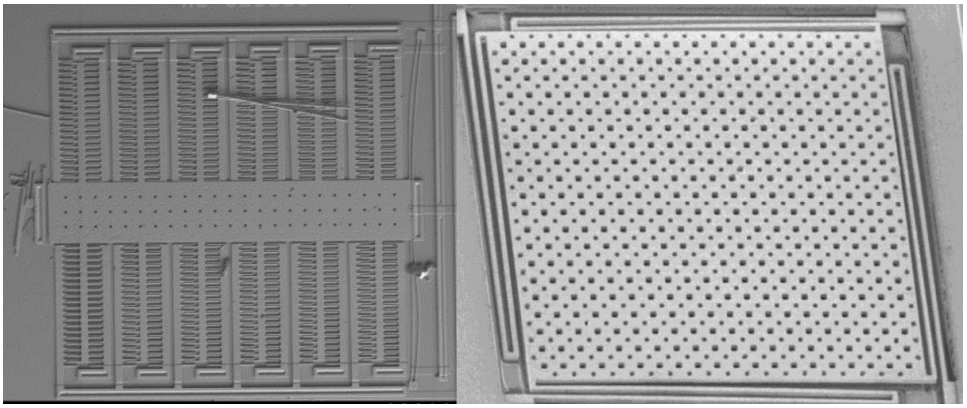

Fig. 2.2. Photos of comb-drive accelerometer (left) [8] and parallel plate accelerometer (right) [9]

2.2. FRINGING FIELD

Let us analyze a parallel plate capacitor, the most commonly used structure in electronic devices. It consists of two plates arranged in parallel. The overlapping surfaces allow to obtain uniform electrostatic field between plates when a voltage is applied on them. In MEMS devices, one of the plates is movable. Thus, the capacitor has variable capacitance. In general, this plate is moving in a direction normal to the plate plane to keep the same overlapping surface during the operation. The capacitance is then calculated with the following equation that takes into account the dimensions of the structure

$$C = \varepsilon \frac{S}{d}, \tag{2.1}$$

where ε is the permittivity of environment, S is the area of plate forming the capacitor and d is the gap distance between plates. However, this formula is valid only for infinitely large parallel plates because it takes into account uniform electric field between plates only. Therefore, devices should have plates as large as possible. In real cases, the electric field exists outside the overlapping surfaces as show in Fig 2.3.

Some works have reported that the real capacitance is almost 45% higher than the value obtained with equation (2.1) [11]. Therefore, equation 1 should be modified in order to take into account the fringing field, which is possible using the definition of capacitance (the ratio of the charge and electric potential). However, it requires solving Maxwell's equation. Thus, alternate methods that makes use of modification of equation (2.1) [12-16] are also available. Note that the influence of fringing field depends on the dimension of the plates (more precisely, the ratio of the length of the plates' edges and plates' area) and gap distance [17]. Second term plays an important role as the gap distance is usually very small and therefore, the results obtained with equation (2.1) are more accurate.

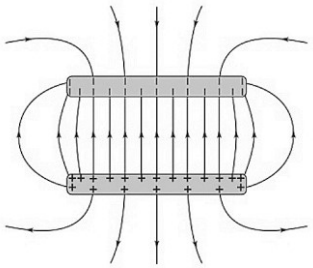

Fig. 2.3. Electric field distribution in parallel plate capacitor

2.3. COMB-DRIVE STRUCTURE

The fringing field effect in comb-drive structure is more complex. Such structure consists of several fingers that forms multiple small capacitors (Fig. 2.4). In addition, there are two capacitors for each finger, the main with small gap and parasitic between each pair of fingers. Although this second gap is much larger, it still plays a role in capacitance (up to 40%). Larger gap distance produces greater impact of fringing field as mentioned in previous paragraph. Additionally, overlapping of combs generate different electric field distribution (Fig. 2.5). In the area between fingers and fixing points, the electric field is closer to linear with rather small distance. Thus, one expects significant impact on the total capacitance.

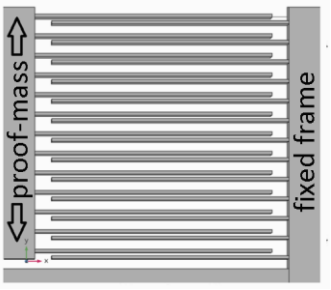

Fig. 2.4. Comb-drive structure in typical *XY*-axis accelerometer

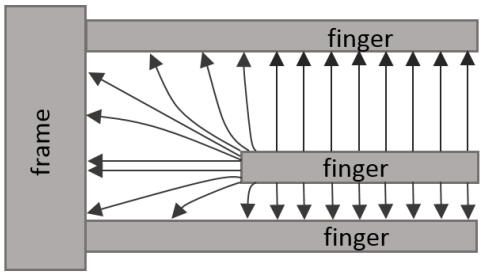

Fig. 2.5. Fringing field in comb-drive structure

The fringing field effect is more complex in the case of *Z*-axis accelerometer. Comb-drive structure is used due to the lack of cavity electrode. The design of such structure is not intuitive. If we redesign the suspension to obtain the deflection of the proof-mass in *Z*-direction, the change in capacitance is independent of the sense of the direction of acceleration. Therefore, such sensors use asymmetrical proof-mass to obtain its rotation [18]. Additional modification is the use of thinned fingers as presented on the X-FAB micromachining process description (Fig. 2.6). Thereafter, two main capacitances are distinguished: each on opposite sides of the sensor (left and right). When the proof-mass rotates in one direction, left combs move down and right combs move up (Fig. 2.7). Due to thinner fingers in the left combs, the corresponding capacitance will decrease while the second one will increase. In the case of opposite direction of proof-mass rotation, the

capacitances also change in the opposite directions respectively. Note that the suspension must be designed in such way to obtain proof-mass twisting. Moreover, suspension bending in Z direction should be negligible.

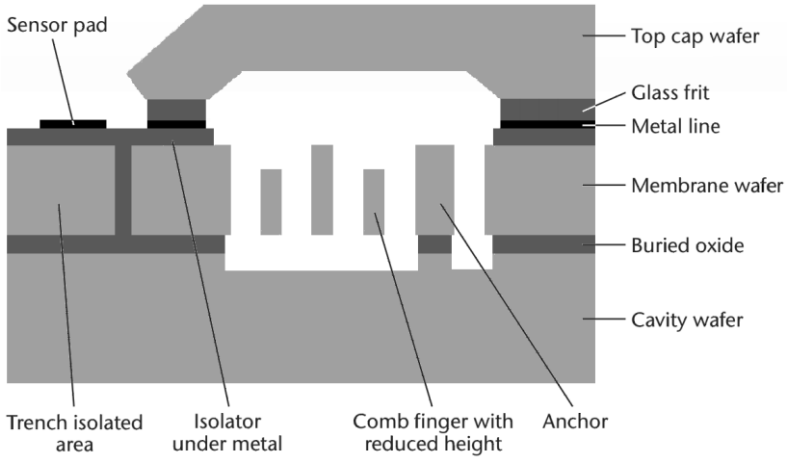

Fig. 2.6. Surface micromachining process cross section [19]

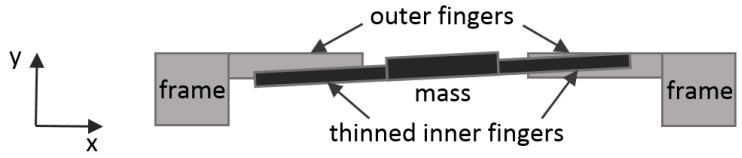

Fig. 2.7. Proof-mass rotation in *Z*-axis accelerometer

2.4. FRINGING FIELD MODELLING

The mechanical description of the sensor is described in [20]. This section will focus on the electrical domain and the computation of the initial capacitance (without acceleration). We start with the previously mentioned equation (2.1). Due to the existence of many fingers, the equation will need to be written in the following form

$$C = n\varepsilon\frac{S}{d}, \tag{2.2}$$

where n is the number of fingers in the inner or outer combs, ε is the permittivity of environment, S is the area of finger forming the capacitor (overlapping surface) and d is the gap distance between fingers. As mentioned earlier, each pair of fingers that form the main capacitance is close enough to the next pair and this capacitance has to be taken into account. Therefore, the capacitance is

$$C = n\varepsilon\frac{S}{d_1} + (n-1)\varepsilon\frac{S}{d_2}, \tag{2.3}$$

where d_1 is the distance between fingers in pair and d_2 is the distance between pairs of fingers (Fig. 2.8). Note that the number of capacitors formed by pair of fingers is one less than the number of capacitors formed by fingers in pairs.

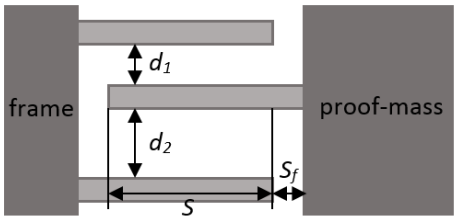

Fig. 2.8. Geometry of capacitors formed by fingers

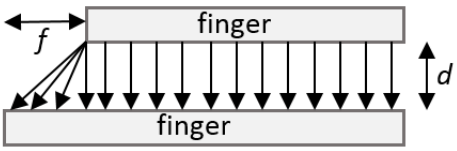

Fig. 2.9. Geometry of capacitors formed by fingers

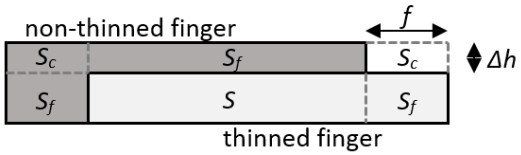

Fig. 2.10. Non-overlapping surfaces in case of thinned fingers

Equation 2.3 allows the calculation of the capacitance that results from the linear electric field between overlapping surfaces (S in Fig. 2.8). Next, the formula for calculating the capacitance resulting from fringing field will be derived. In order to simplify the calculations, suitable assumptions will need to be made. The electric field for non-overlapping area S_f is assumed to be linear as shown in Fig. 2.9. Thereafter, we can calculate the mean distance d_m between fingers and use classical formula for capacitance (equation 2.1) as follows

$$C_f = \varepsilon \frac{S_f}{d_m}, \quad d_m = 0.92 \frac{d + \sqrt{d^2 + f^2}}{2}, \tag{2.4}$$

where f is the length of non-overlapping part of the finger. The constant 0.92 in equation (2.4) is set experimentally as the calculation of the exact mean value is complicated. This value is correct for ratio f/d up to 10 (typical in most accelerometers). Equation (2.4) has to be used for all non-overlapping surfaces, those corresponding to fingers and those corresponding to proof-mass and frame. Note that in case of Z-axis accelerometer, additional non-overlapping surfaces exist due to fingers thinning. All non-overlapping surfaces are marked in Fig. 2.10. In case of corner areas S_c, the calculation is made in a similar way as previously described using the following formulas

$$C_c = \varepsilon \frac{S_c}{d_{mc}}, \quad d_{mc} = 0.92 \frac{d + \sqrt{d^2 + f^2 + \Delta h^2}}{2}, \tag{2.5}$$

where d_{mc} is the mean value and Δh is the difference in the height between fingers.

2.3. RESULTS AND COMPARISON WITH MEMS+

In our previous works, we designed *XY*-axis and *Z*-axis accelerometers [17, 20]. These accelerometers are designed in compliance with X-FAB technology [19]. Thus, the thickness of sensor layer is 30 μm and all accelerometers use comb-drive structure. *Y*-axis accelerometer uses H-shape proof-mass with four springs on each ending. This shape allows placing the combs outside and inside the proof-mass. The thickness of fingers is as small as possible in this technology (2 μm). Its length is 75 times larger (technological limit). The distance between fingers is 2 μm (as small as possible) in order to obtain high initial capacitance. The distance between each pair of fingers is set to 6 μm to minimize undesirable electrostatic force between these fingers. Separation distance between fingers and fixing points is set to 10 μm. *X*-axis accelerometer has the same structure but scaled with a factor of 1.5. The idea was to investigate the behavior of the sensor with higher sensitivity but with possible non-linear response. *Z*-axis accelerometer differs significantly due to the rotational response of the sensor. The main dimensions of fingers are taken from *X*-axis accelerometer to obtain higher sensitivity as the use of asymmetrical proof-mass reduces the total number of fingers – only outside combs may be placed. The height of thinned fingers is 20 μm. The suspensions use only two springs connected on opposite sides of the proof-mass in its axis of rotation. The total size of the sensor is similar to *Y*-axis accelerometer. All sensor dimensions are shown in Table 2.1.

Table 2.1. Accelerometers dimensions

	Y-axis	*X*-axis	*Z*-axis
Finger length	140 μm	200 μm	200 μm
Finger width	2 μm	4 μm	4 μm
Finger separation	10 μm	15 μm	10 μm
Sensor layer thickness	30 μm		
Thinned finger thickness	not used	20 μm	
Gap between fingers	2 μm		
Gap between pairs of fingers	6 μm		
Number of finger (per side)	56	80	52

These accelerometer models have been implemented in MEMS+ as shown in Fig. 2.11. Next, DC analysis has been run in order to calculate the initial capacitance of the structure. In case of analytical calculation, the results are presented for each component separately: parallel plate capacitance eq. (2.3), capacitance due to fringing field for each non-overlapping surface eq. (2.4 and 2.5) and capacitance between fingers endings and frame/proof-mass eq. (2.2). Note that the capacitance is calculated for both gap distances: 2 μm and 6 μm.

The results for *Y*-axis accelerometer are presented in Table 2.2. One has to observe that it is necessary to take into account the capacitance between each pair of fingers. Gap distance between them is only a few times larger than the one between fingers in pair.

In our case, it is about 25% of total capacitance. Capacitance due to fringing field is calculated to be about 5%. In comparison to MEMS+, analytical model is underestimated by 5%. It is understandable because no fringing field along overlapping fingers is taken into account. Estimations show that parallel plate capacitance should be increased by about 5% to cover the difference.

Table 2.2. Results for *Y*-axis accelerometer

Y-axis accelerometer		Capacitance [pF]		
		Analytical model		MEMS+
Parallel plate	*d*=2 µm	0.966	1.012	–
Separation fringing field		0.046		
Parallel plate	*d*=6 µm	0.316	0.343	
Separation fringing field		0.027		
Fingers endings		0.021		
Total capacitance		1.376		1.446

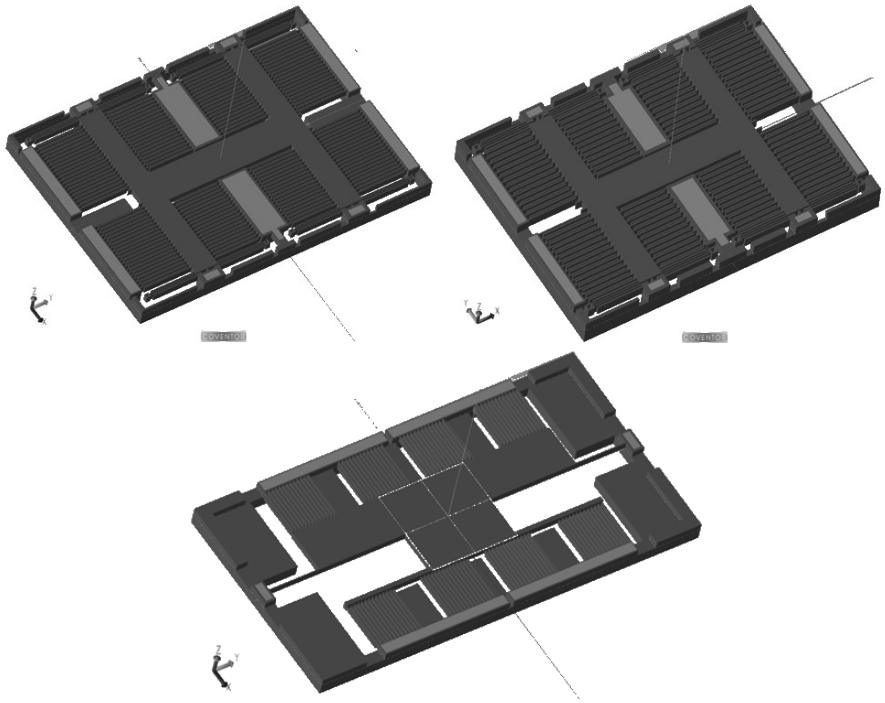

Fig. 2.11. Accelerometer models in MEMS+: *X*-axis (top-left), *Y*-axis (top-right) and *Z*-axis (bottom)

Next, *X*-axis accelerometer was analyzed. The results are presented in Table 2.3. The results are similar to the previous accelerometer. Fringing field for non-overlapping surfaces play a smaller role as separation distance is the same with 1.5 times longer fingers. This results also in larger difference compared to MEMS+ results. Now, analytical model is underestimated by about 10%. Parallel plate capacitance should be increased by about 12%. Note that in this case, finger width is two times larger. Thus, the capacitance due to fringing field for overlapping surfaces is larger than in *Y*-axis accelerometer.

Table 2.3. Results for *X*-axis accelerometer

X-axis accelerometer		Capacitance [pF]		
		Analytical model		MEMS+
Parallel plate	*d*=2 µm	1.964	2.036	–
Separation fringing field		0.072		
Parallel plate	*d*=6 µm	0.647	0.696	
Separation fringing field		0.049		
Fingers endings		0.025		
Total capacitance		2.757		3.07

Finally, *Z*-axis accelerometer was analyzed. The results are presented in Table 2.4.

Table 2.4. Results for *Z*-axis accelerometer.

Z-axis accelerometer		Capacitance [pF]		
		Analytical model		MEMS+
Parallel plate	*d*=2 µm	0.874	1.047	–
Thinned fingers fringing field		0.133		
Separation fringing field		0.028		
Corner fringing field		0.011		
Parallel plate	*d*=6 µm	0.286	0.390	
Thinned fingers fringing field		0.080		
Separation fringing field		0.017		
Corner fringing field		0.007		
Fingers endings		0.014		
Total capacitance		1.451		1.444

As seen, fringing field due to thinned fingers was taken into account in this case. The capacitance is then increased by about 18%. The total capacitance is now almost the same as the one obtained in MEMS+ although the fringing field between one of the finger edges (those in the same plane) is not taken into account. However, the capacitance due to thinned fingers fringing field is overestimated. Analytical model assumes that electric field lines are straight. Therefore, the mean distance is overestimated.

2.4. EXPERIMENTAL VERIFICATION

All of the above-mentioned accelerometers have been fabricated using X-FAB XMB10 MEMS technology. Each type of accelerometer has been placed on separate wafers. One of them is presented in Fig. 2.12. Note that this technology uses top cap wafer in bonding process. Thus, accelerometers are encapsulated and only test structures with bonding pads are visible. In the measurement of initial capacitance, FormFactor Summit 11000 probe station is used where, probes are connected to pads corresponding to capacitance terminals. Probes are connected to Keysight E4990A probe analyzer that allows the measurement of capacitance in the range of pF.

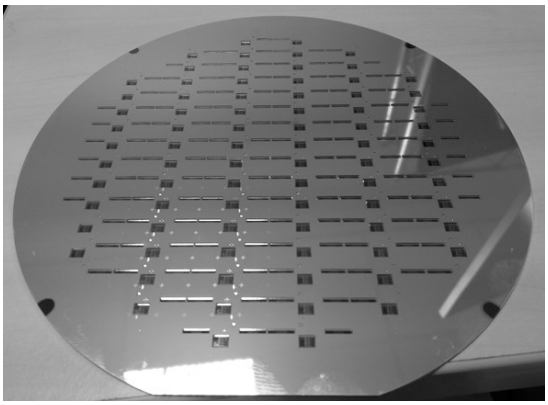

Fig. 2.12. Wafer fabricated using X-FAB technology

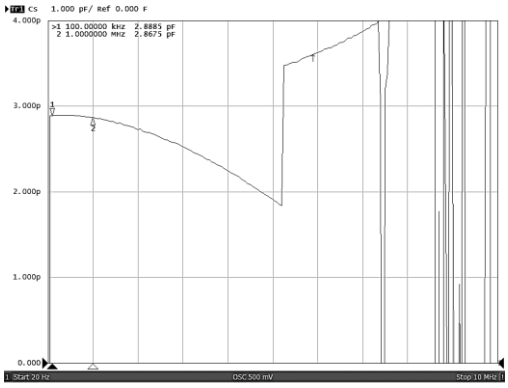

Fig. 2.13. Initial capacitance measurement for *X*-axis accelerometer

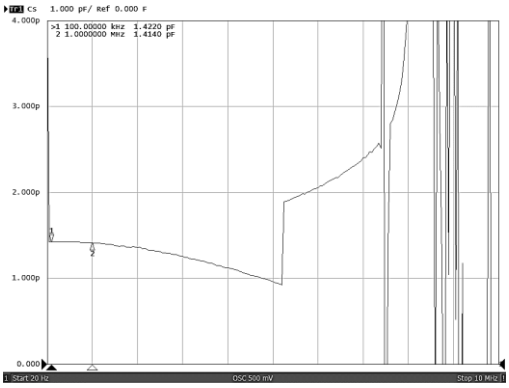

Fig. 2.14. Initial capacitance measurement for *Y*-axis accelerometer

Several structures have been measured for each type of accelerometer. Exemplary results are presented in Fig. 2.13–2.15. Initial capacitance for *X*-axis accelerometers is in the range 2.888–2.898 pF, for *Y*-axis accelerometers in the range 1.421–1.424 and for *Z*-axis accelerometers, in the range of 1.386–1.399. As seen, the measured values are very close to those obtained with MEMS+. In real device, the encapsulation and bottom wafer disturbs the electric field and influences the capacitance. Nevertheless, this impact seems to be negligible because results obtained with MEMS+ are slightly overestimated. Note that the measurement accuracy of impedance analyzer is very high (error smaller than 1%) and does not compensate the difference. In the case of *Y*-axis accelerometer, the difference is 2%, while in the case of *X*-axis and *Z*-axis accelerometers, the difference rises to 5%. It seems that MEMS+ overestimates for larger structures. However, it is possible that some mismatch results from technological process even though the measurements are very repetitive. Nevertheless, both MEMS+ results and experimental results show that analytical model gives quite accurate results.

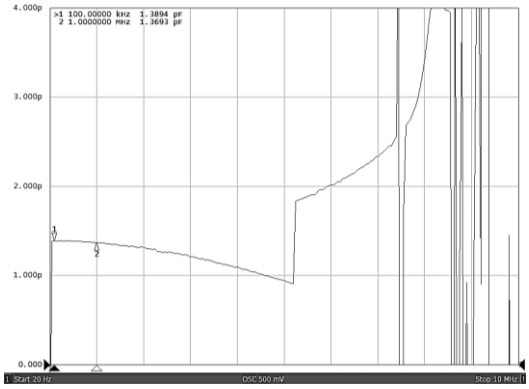

Fig. 2.15. Initial capacitance measurement for *Z*-axis accelerometer

2.5. CONCLUSIONS

In this chapter, modeling approaches of MEMS accelerometers have been described with particular reference to phenomena that may affect the precision of the results. One of the most significant considerations in capacitive structures is the fringing field. Its influence on capacitance was discussed considering the example of comb-drive structure that consists of many small parallel plate capacitors. Therefore, fringing field in such structures has to be modelled properly. In our model, the capacitance resulting from fringing field is calculated for non-overlapping surfaces using simplification that assume that the field lines are straight. The results have been compared with those obtained with MEMS+ for three types of accelerometers: *X*-axis, *Y*-axis and *Z*-axis. Analytical model is underestimated by about 5–10% and gives almost the same results for *Z*-axis accelerometer. It has been found that analytical model overestimates capacitance resulting from fringing field and therefore additional non-overlapping surface for thinned fingers in *Z*-axis accelerometer compensates the difference. In addition, it has been observed how analytical model may be simply improved to increase precision. Nevertheless, analytical model gives accurate results that can be used in the early stage of the project or in optimization phase to reduce the simulation time. One has to emphasize that the final results should be verified with a more precise simulator (MEMS+ or classical FEM simulation used in ANSYS, COMSOL). Finally, simulated structures have been fabricated and measured. Results obtained from measurements correspond to those obtained from simulations and proves that analytical model is a very efficient method in prototyping phase.

Results presented in the chapter are supported by the project STRATEGMED 2/266299/19NCBR/2016 funded by The National Centre for Research and Development in Poland.

REFERENCES

[1] ANDREJAŠIC M., *MEMS Accelerometers*, University of Ljubljana, http://mafija.fmf.uni-lj.si/seminar/files/2007_2008/MEMS_accelerometers-koncna.pdf (accessed: 11.05.2020).

[2] *Technavio Global MEMS Accelerometer Market 2015-2019*, https://www.technavio.com/report/global-mems-accelerometer-market-2015-2019 (accessed: 11.05.2020).

[3] FRADEN J., *Handbook of Modern Sensors*, Springer, New York, 2010.
[4] KORVINK J., PAUL O., *MEMS: A Practical Guide of Design, Analysis, and Applications*, Springer Berlin Heidelberg, 2006.
[5] CHOUDHARY V., INIEWSKI K., *MEMS: Fundamental Technology and Applications*, CRC Press, 2017.
[6] MAJ C. et al., A Multi-domain Electrostatic Actuator Design Tool based on Analytical Models, in: *Proc. International Conference MIXDES*, Gliwice, Poland, 2011.
[7] OLSZACKI M. et al., A multi-domain piezoresistive pressure sensor design tool based on analytical models, in: *Proceeding of 9th International Conference on Thermal, Mechanical and MultiPhysics Simulation and Experiments in Microelectronics and Microsystems (EuroSimE 2008)*, Freiburg, 2008.
[8] SZANIAWSKI K., *Projektowanie i symulacja scalonych czujników wibracji i przyspieszenia*, PhD dissertation at Lodz University of Technology, 2005.
[9] MAJ C. et al., Macro Model of Capacitive MEMS Accelerometer in Cadence Environment, in: *Proceeding of 17th International Conference on Thermal, Mechanical and MultiPhysics Simulation and Experiments in Microelectronics and Microsystems (EuroSimE)*, Montpellier, France, 2016.
[10] KANNAN A., *Design and modeling of a MEMS-based accelerometer with pull in analysis*, MASc dissertation, University of British Columbia, 2008.
[11] PARKER G. W., What is the Capacitance of Parallel Plates?, *Computers in Physics*, vol. 5(5), p. 534-540, 1991.
[12] GALLAGHER E., MOUSSA M., A Study of the Effect of the Fringe Fields on the Electrostatic Force in Vertical Comb Drives, *Journal of Sensors*, vol. 14, 2014.
[13] HOSSEINI M., ZHU G., A new formulation of fringing capacitance and its application to the control of parallel-plate electrostatic micro actuators, *Journal of Analog Integrated Circuits and Signal Processing*, vol. 53, p. 119–128, 2007.
[14] BURT S., FINNEY N., YOUNG J., *Fringe Field of Parallel Plate Capacitor*, Santa Rosa Junior College.
[15] WIAK S., SMÓŁKA K., Numerical modeling of 3-D comb drive electrostatic accelerometers structure (method of levitation force reduction), *COMPEL International Journal of Computations and Mathematics in Electrical*, 2009.
[16] CHEN X., ZHANG Z. et al., Fringing Effect Analysis of Parallel Plate Capacitors for Capacitive Power Transfer Application, in: *4th IEEE International Future Energy Electronics Conference, IFEEC 2019*, Singapore, 2019.
[17] MAJ C., SZERMER M., JANKOWSKI M., Influence of Fringing Field on Estimating of Comb-Drive Accelerometer Performance Comb-drive Accelerometer Performance, in: *Proc. of XVth International Conference on Perspective Technologies and Methods in MEMS Design (MEMSTECH)*, Polyana-Svalyava, Ukraine, 2019.
[18] MAJ C., SZERMER M., Designing of Z-axis comb-drive MEMS accelerometer, in: *Proc. of XXVI International Polish-Ukrainian Conference CAD in Machinery Design: Implementation and Educational Issues (CADMD)*, Lviv, Ukraine, 2018.
[19] https://www.xfab.com/fileadmin/X-FAB/Download_Center/Technology/MEMS/is_XMB10_MEMS_3-Axis_Inertial_Sensors_May2017.pdf (accessed: 11.05.2020).
[20] SZERMER M., ZAJĄC P. et al., Influence of Geometry Scalling on Comb-drive Accelerometer Performance, in: *Proc. of XIVth International Conference on Perspective Technologies and Methods in MEMS Design (MEMSTECH)*, Polyana-Svalyava, Ukraine, 2018.
[21] MAJ C., SZERMER M., Designing of Z-axis accelerometer with asymmetric proof-mass using surface micromachining process, in: *Proc. of 15th International Conference of Experience of Designing and Application of CAD Systems in Microelectronics CADSM 2019*, Polyana-Svalyava, Ukraine, 2019.